LETTER TO THE EDITOR

On the realization of artificial XY spin chains

INSTITUTE OF PHYSICS PUBLISHING JOURNAL OF PHYSICS: CONDENSED MATTER

J. Phys.: Condens. Matter **17** (2005) L27–L33 doi:10.1088/0953-8984/17/2/L04

LETTER TO THE EDITOR

On the realization of artificial XY spin chains

M van Kampen[1], I L Soroka[1,6], R Bručas[1], B Hjörvarsson[1], R Wieser[2], K D Usadel[2], M Hanson[3], O Kazakova[3], J Grabis[4], H Zabel[4], C Jozsa[5] and B Koopmans[5]

[1] Fysiska Institutionen, Box 530, 751 21 Uppsala, Sweden
[2] Universität Duisburg-Essen, Germany
[3] Chalmers University of Technology, Göteborg, Sweden
[4] Ruhr-Universität Bochum, Germany
[5] Center for NanoMaterials and COBRA Research Institute, Eindhoven University of Technology, The Netherlands

E-mail: inna.soroka@fysik.uu.se

Received 2 December 2004, in final form 2 December 2004
Published 20 December 2004
Online at stacks.iop.org/JPhysCM/17/L27

Abstract

Spin chains are the most elementary entities in the study of magnetic ordering behaviour. In this letter, we describe a route toward the realization of artificial XY spin chains. Using thin-film deposition and e-beam lithography, 300 and 550 nm diameter pillars consisting of alternating discs of permalloy and Al_2O_3 have been made. Shape anisotropy forces the magnetization in plane, creating a chain of two-dimensional magnetic moments $\vec{S}_i$. The discs couple to each other by their dipolar stray fields, resulting in an interaction of the form $J_{ij}\vec{S}_i \cdot \vec{S}_j$, with J_{ij} the coupling between discs i and j. This form closely resembles a chain of xy spins, coupled by effective interactions J_{ij}. We present a magnetic characterization of the pillars, and compare the results with model calculations. Also, spin dynamics and ordering phenomena are addressed.

Spin chains are the most basic elements in the description of magnetic ordering phenomena. Due to their relative simplicity, the properties of such chains are well known from theory. So far, approximations of this idealized configuration have only been obtained experimentally in long molecules [1] and in bulk compounds that, by their crystallographic structure, show chains of magnetic moments [2–4]. Only very recently, ordering in an 'artificial' chain structure has been investigated [5]. In the latter work, monatomic magnetic chains were formed by Co atoms decorating step edges of a Pt substrate. Potential advantages of the use of artificial spin chains lie in a better control of chain length, a larger freedom in the choice of magnetic materials, and a greater flexibility in tuning of the coupling interactions.

[6] Author to whom any correspondence should be addressed.

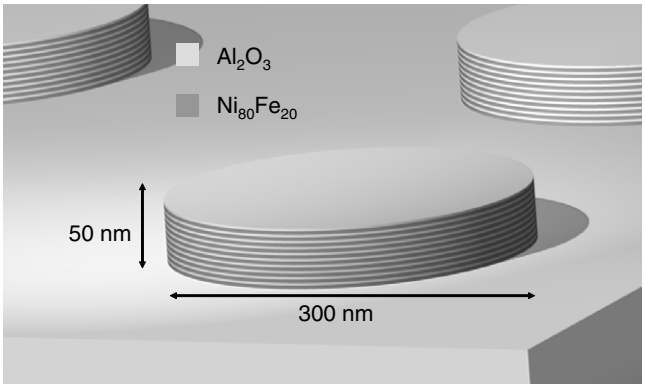

Figure 1. Schematic picture of the pillar structures. The bright discs represent Al_2O_3 (1.8 nm thick), the dark discs permalloy (3.0 nm thick). The total structure consists of 10 permalloy/Al_2O_3 repeats, resulting in a total height of ∼50 nm.

In this letter we describe the fabrication and characterization of lithographically defined spin chains. Using lithography, stacks of permalloy ($Ni_{81}Fe_{19}$) discs with diameters of 300 and 550 nm have been created. The permalloy discs are separated by non-magnetic spacers, thus forming isolated magnetic entities or 'spins', cf figure 1. Choosing Al_2O_3 as an insulating spacer material, the coupling between the discs is fully mediated by the dipolar stray field. Therefore, the (vertical) chains are expected to show an anti-ferromagnetic (AF) ground-state. Alternatively, one can use a metallic spacer. This introduces an RKKY type of coupling, also allowing for a ferromagnetic ground state.

In the following, we describe the fabrication and structural characterization of the elements. Next, their magnetic properties are presented and compared with a theoretical model. Finally, we present preliminary results on their spin-dynamics behaviour and comment on the applicability of this type of structures to the study of ordering phenomena.

The spin-chain structures were fabricated from a uniform $Al_2O_3/Ni_{81}Fe_{19}$ multilayered film, using electron-beam lithography and ion-beam milling. The multilayer film was deposited in an Ar environment (2×10^{-3} Torr) on an oxidized Si(001) substrate using dc and rf magnetron sputtering of permalloy and Al_2O_3 targets, respectively. The structural properties of the prepared film were checked *ex situ* by x-ray diffraction (XRD) and transmission electron microscopy (TEM), allowing for a precise determination of the thickness and interface quality of the constituent layers. Next, the uniform film was patterned using e-beam lithography, writing in 1×1 mm^2 areas of resist. After exposure and development, excess material was removed by ion-beam (Ar^+) milling, resulting in structures with well defined lateral geometry and high aspect ratio. Using the above procedure, arrays of 300 and 550 nm diameter pillars have been created, with a centre-to-centre distance of 0.6 and 1.0 μm, respectively. Every pillar consists of ten repeats of $Ni_{81}Fe_{19}$(3.0 nm) and Al_2O_3(1.8 nm) alternating layers, starting and ending with an amorphous Al_2O_3 layer to ensure a polycrystalline growth and to prevent oxidation.

The magnetic properties of the films and structures were characterized using magnetic force microscopy (MFM) and the magneto-optic Kerr effect (MOKE). In figure 2(a) results of measurements on the unpatterned multilayer are presented. The unpatterned films show a high remanence and a very low coercivity of 0.1 mT, as is characteristic for polycrystalline permalloy. Surprisingly, a relatively strong uniaxial anisotropy is present, resulting in a hard axis showing a 1 mT saturation field. As the sample was rotated during growth, a field-induced

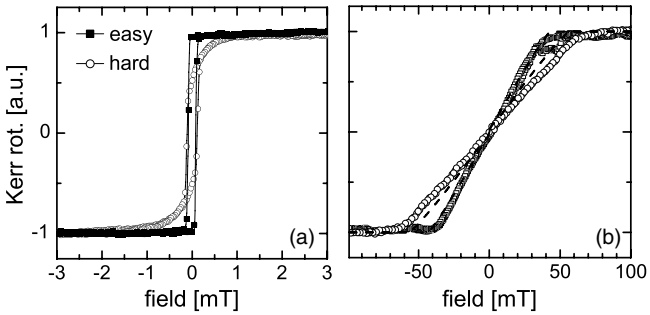

Figure 2. Magnetization loops on the unpatterned (panel (a)) and patterned (panel (b)) films. The unpatterned films are saturated in a 0.1 mT (easy axis) or 1 mT (hard axis) field. After patterning, fields of 60 and 43 mT are needed to saturate the 300 and 550 nm diameter structures, respectively. The dotted lines in panel (b) represent calculated curves.

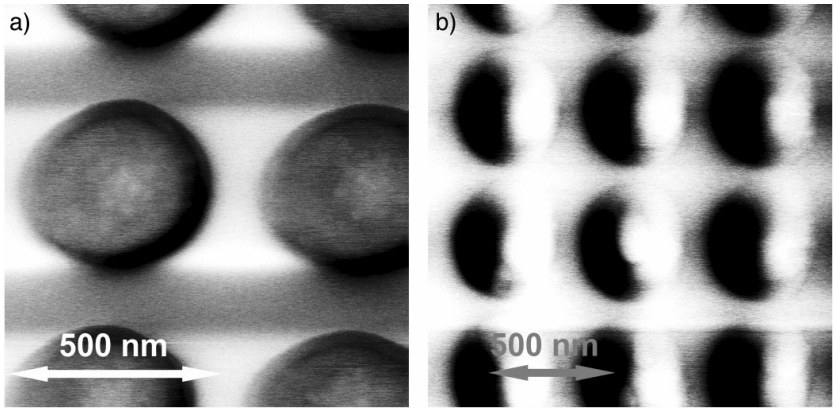

Figure 3. MFM scans of the 300 nm diameter array. (a) Remanent state; the horizontal bands are a scanning artifact. (b) ∼30 mT in-plane field. The induced dipole moment in each pillar results in a black–white contrast.

anisotropy can be excluded. More likely, strain and magnetoelastic effects are responsible for the observed anisotropy. Although bulk permalloy shows a very small magnetostriction, it has been shown that for thin films (<7 nm) strong magnetostriction effects can occur [10].

After patterning a completely different picture emerges, cf figure 2(b). In zero applied field, no net magnetic moment is present. Upon applying an external field, the magnetization increases until it saturates at 60 and 36 mT, respectively, for the 300 and 550 nm diameter structures. These numbers can be compared with the saturation fields of less than 1 mT of the unpatterned film. No in-plane anisotropy could be detected. The behaviour of the structured film can be understood by assuming an anti-ferromagnetic coupling between neighbouring discs in a pillar. At zero field the magnetic moments of the (even number of) discs completely compensate, while with increasing the field the discs start to align and give rise to a net magnetic moment.

In figure 3 MFM scans on the 300 nm diameter array are shown. The scan in panel (a) was made without external field, i.e. in the remanent state. The observed lack of magnetic contrast is expected for an AF ground state, as flux closure strongly reduces stray fields. Note that the MFM scan also excludes a vortex state. Panel (b) shows a scan in an in-plane field of ∼30 mT.

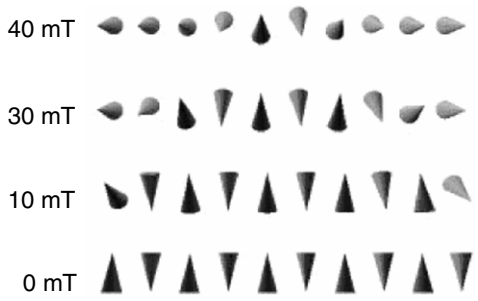

Figure 4. Spin configuration for the 550 nm diameter structures at selected fields, with the field applied out of the page. At 0 mT, neighbouring discs align anti-parallel. Increasing the field, the outer spins are the first to align as they are most weakly coupled.

The external field induces a net moment in each individual pillar, resulting in a typical dipolar contrast.

This interpretation is supported by results obtained from numerical simulations. In the calculations it is assumed that inter-pillar coupling is negligible and that the magnetization in the discs is strictly within the plane, free to rotate and homogeneous. These are reasonable assumptions for the current structures. The spacing between the pillars is large, and no in-plane anisotropy was observed for the patterned structures. Shape anisotropy forces the magnetization in plane since the 'pillars' are still much wider (lateral dimensions down to 300 nm) than high (total thickness of 50 nm). Since the magnetic discs consist of polycrystalline permalloy, showing a very low anisotropy, the magnetization can (almost) freely rotate. The assumption of a homogeneous magnetization deserves special attention. It is well known that vortex states can occur in circular microstructures [6]. Their occurrence depends on the ratio of thickness to diameter and the exchange length [8, 7]. From the phase diagram in [7], and from our own micromagnetic calculations [9], it can be concluded that each isolated magnetic disc is already single domain. In the pillar structures, the AF alignment between the discs will greatly reduce the stray field, and thus remove the drive for vortex formation. Additionally, no vortices were observed in the MFM scans.

To calculate the stray-field coupling, we decompose the discs in a pillar into small cells of extension $(2\ \mathrm{nm})^3$ and replace the (in-plane) magnetic moment of each cell by a point dipole. Since these dipoles are all parallel within the discs it is easy to calculate the net dipolar interaction between discs. The resulting interaction between the magnetic moments of different discs is of the Heisenberg type,

$$H = J(d_{ij})\vec{S}_i \cdot \vec{S}_j, \tag{1}$$

so that we finally end up with a chain of spins coupled by effective interactions $J(d)$. Its ground-state properties have been calculated numerically and the result for the magnetization component parallel to the external field is shown in figure 2(b) (dotted lines), together with the experimental data. The calculated magnetization curves show saturation fields of 43 and 55 mT, for the 300 and 550 nm diameter pillars, respectively. This in excellent agreement with the experimental values of 36 and 60 mT. Note that the only input to the model is the dimension of the discs and the magnetization of permalloy, taken to be 732 kA m^{-1}. In figure 4, the calculated magnetization vectors of the ten discs in the 550 nm diameter structure are depicted for different fields. At 0 mT one finds a perfect AF alignment, while for increasing fields the discs gradually align with the field. Since the outermost discs lack neighbours, they are less strongly coupled and align more easily with the applied field.

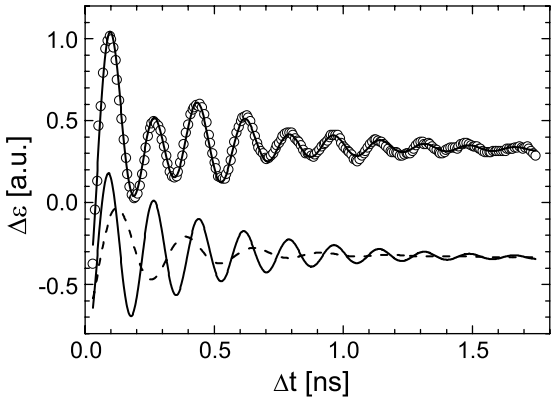

Figure 5. Precessing magnetization vector in the 300 nm diameter pillars. The open circles represent the time dependence of the Kerr ellipticity $\Delta\epsilon$, proportional to the a weighted average of the out-of-plane magnetization of the permalloy discs. The data are well described by a sum of two damped sines (solid curve; separate contributions are shown below), with frequencies of 5.7 and 3.8 GHz. During the measurement, a field of 2.5 kG was applied at an angle of $\approx 10^\circ$ with respect to the film normal.

The dipolar coupling between the ten discs is also expected to affect the magnetization dynamics, showing up as a discrete spectrum of spin-wave excitations. These excitations can be seen as a variant of perpendicular standing spin waves, i.e. standing modes in the thickness of a film. However, in this case only ten discrete moments contribute. For a spin chain, thermal population of these modes will break the AF order with increasing temperature. First evidence for these inter-disc dipolar modes comes from time-resolved magnetization measurements. Using an all-optical technique described in detail in [12], the precessing magnetic moment can be followed in time after sudden laser excitation. Since due to absorption both the optical excitation and the optical detection are non-uniform within the height of the pillar, higher-order standing modes can be excited and detected. First results are shown in figure 5, where the open circles represent the measured change in Kerr ellipticity as a function of time after excitation. Using near-perpendicular incidence, this signal is proportional to a weighed average of the out-of-plane magnetization of the ten discs in each pillar. The oscillating signal therefore represents the out-of-plane component of the precessing magnetization in the discs. On closer inspection, two discrete modes can be discerned with precession frequencies of 5.7 and 3.8 GHz. Although the results are preliminary, first indications are that the high-frequency mode corresponds to the uniform precession (acoustical mode), and the low-frequency mode to a higher-order excitation (optical mode). This is exactly the order that is expected for an AF coupled system.

Note that coupling between the discs is not the only mechanism resulting in a discrete spectrum. Alternatively, one can have standing spin waves inside a single disc. Since the individual discs are only 3 nm thick, perpendicular standing spin waves should have much higher frequencies than the $\sim$6 GHz observed. Lateral standing waves can also result in a discrete spectrum; see e.g. [11]. However, in the current experiments a laterally extended ($\varnothing 10$ μm) laser spot is used. The 300 nm diameter pillars will therefore be both uniformly excited and uniformly probed in the lateral dimensions, suppressing the excitation and detection of lateral modes.

The motivation behind this work is the creation of a model system in the study of magnetic ordering phenomena: a spin chain. The structures created thus far do indeed closely resemble a chain of coupled xy moments; see e.g. equation (1). However, to truly approach the model

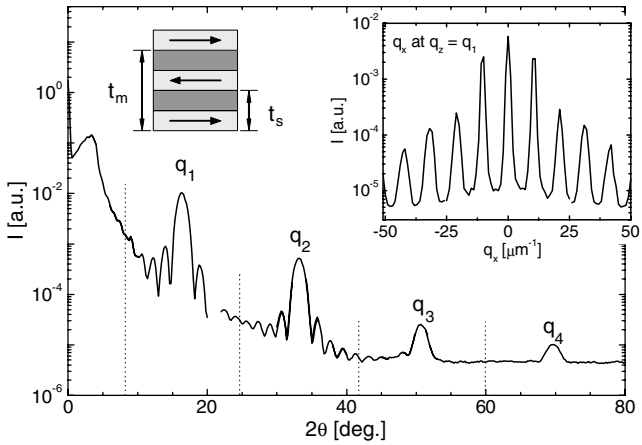

Figure 6. θ–2θ scan on the 300 nm diameter pillar structure using 853 eV (Ni L3-edge) synchroton radiaton. The four peaks labelled q_1 to q_4 correspond to the structural Bragg peaks (t_s in the inset). No features are observed near the dotted lines indicating the expected positions of the AF Bragg peaks, i.e. corresponding to the AF unit cell $t_m = 2t_s$. Inset: q_x scan at the first Bragg peak, showing the interference due to the 0.6 μm spacing between the pillars.

system and to be able to study the thermodynamics of the order–disorder transitions in a spin chain, the individual discs should behave as macro-spins. This condition is met in the superparamagnetic limit: when the volume of a magnetic element is sufficiently small, thermal excitations can overcome the barrier for switching of the magnetization. For soft-magnetic materials, this volume can be reached with current lithography techniques. In [13], the onset of superparamagnetism in nanostructures is studied as a function of shape, size and thickness. Using supermalloy, a soft-magnetic alloy, 3 nm thick hexagonal structures showed the onset of (room-temperature) superparamagnetism for a lateral dimension of 200 nm. Apart from a decrease in lateral dimension, an increase in magnetic softness can also trigger a transition to a superparamagnetic state. Possible routes to the realization of a true thermodynamic model system therefore include a further reduction of the lateral dimensions, and the use of extremely soft magnetic materials, e.g. amorphous alloys.

To study the magnetic order in the stack, experimental techniques are required that can measure the AF order parameter,

$$q_{1/2} = \left[\tfrac{1}{10} \sum_{n=1}^{10} (-1)^n S_{x,i} \right]^2 , \tag{2}$$

with $S_{x,i}$ the x component of the magnetization of disc i. For this purpose, spin-resolved neutron scattering and resonant x-ray reflectivity are candidates. However, due to the low effective coverage of only 0.3 mm^2, the signal-to-noise ratio in neutron experiments will be insufficient. Using intense synchrotron radiation, satisfactory measurements can be made. Figure 6 shows a theta–two theta scan on the 300 nm diameter structure using circularly polarized synchroton radiation at the Ni L3 edge (853 eV). At this edge, magneto-optic effects are strongly enhanced, allowing one to probe the magnetic order. The structural Bragg peaks, labelled q_1 to q_4 and corresponding to a repetition length $t_s \approx 5$ nm, are clearly visible in the figure. For an AF ordered stack, the magnetic repetition length t_m is twice the structural one. However, no features can be discerned at the positions in q space corresponding to t_m, indicated by the dotted lines. This is most likely caused by the large coherence area of the synchrotron

radiation, combined with a twofold degeneracy of the lowest-energy state. In a small field H_y, the magnetization of each bottom disk can point in two directions, $S_{x,1} = \pm 1$. Since there is no way to control this orientation with an external field, $S_{x,1}$ will vary stochastically between the pillars. Due to the large coherence area of the x-rays, the information on the AF order is averaged out between the pillars. One should therefore revert to techniques having a much smaller coherence area, e.g. neutron scattering, or use a pinning layer and thereby lift the degeneracy. Then, the temperature-dependence of the amplitude of the AF peaks can be taken as a measure of the AF order in the pillars. Note that the lateral order of the structure can also be mapped by performing an off-specular scan. In the inset of the figure, a q_x scan at the first Bragg peak is shown, revealing the 0.6 μm spacing between the pillars.

Concluding, we have fabricated pillars consisting of alternating discs of permalloy and Al_2O_3. Dipolar coupling between the magnetic discs results in an AF ground state, and a Hamiltonian closely resembling that of an xy spin chain. The AF ground state is confirmed by model calculations and experimental magnetization loops. At the length-scale used here, the magnetic discs do not behave as macro-spins. A further reduction of dimensions, or an increase in magnetic softness, is required to pass the superparamagnetic limit. Experimentally, the temperature dependence of the AF order can be studied with resonant x-ray reflectivity. Using the latter technique, the magnetization of the top or bottom spin should be fixed to lift the twofold degeneracy of the lowest-energy state. Otherwise, stochastic fluctuations in the configuration of different pillars within the coherence area of the radiation will average out the AF peak.

Financial support from the Swedish Research Council (VR), STINT and the Swedish Foundation for Strategic Research (SSF) is acknowledged. The groups in Duisburg and Bochum would like to acknowledge financial support through the DFG Sonderforschungsbereich (SFB) 491. HZ and JG also acknowledge support for the synchotron work through BMBF 03ZA6BC2.

References

[1] Affronte M, Pini M G, Rettori A and Sessoli R 1999 *Phys. Rev.* B **59** 6282
[2] de Jongh L J and Miedema A R 1974 *Adv. Phys.* **23** 1
[3] Steiner M, Villain J and Windsor C G 1976 *Adv. Phys.* **25** 2
[4] Mikeska H J 1979 *J. Magn. Magn. Mater.* **13** 35
[5] Gambardella P *et al* 2002 *Nature* **416** 301
[6] Dennis C L *et al* 2002 *J. Phys.: Condens. Matter* **14** R1175
[7] Dau N, Whittenburg S L and Cowburn R P 2001 *J. Appl. Phys.* **90** 5235
[8] Cowburn R P, Koltsov R K, Adeyeye A O, Welland M E and Tricker D M 1999 *Phys. Rev. Lett.* **83** 1042
[9] http://math.nist.gov/oommf NIST's micromagnetics package
[10] Kim Y K and Silva T J 1996 *Appl. Phys. Lett.* **68** 2885
[11] Demokritov S O, Hillebrands B and Slavin A N 2001 *Phys. Rep.* **348** 441
[12] van Kampen M *et al* 2002 *Phys. Rev. Lett.* **88** 227201
[13] Cowburn R P, Koltsov D K, Adeyeye A O and Welland M E 2000 *J. Appl. Phys.* **87** 7082